Noise-source turbulence statistics and the noise from a Mach 0.9 jet

J. B. Freund
Theoretical and Applied Mechanics, University of Illinois at Urbana-Champaign, Urbana, Illinois 61801

(Received 7 October 2002; accepted 5 March 2003; published 6 May 2003)

Turbulence statistics that are relevant to jet noise modeling but difficult to measure in experiments are computed using a previously validated simulation database of a Mach 0.9 cold jet. Initial focus is on fourth-order statistics that are at the core of acoustic analogy based models built on both the Lilley and Lighthill equations. Common simplifications of fourth-order correlations based on normal statistics are found to be accurate. We see that although two-point correlations are well fitted by exponential functions, as is typical of turbulence at all but the lowest Reynolds numbers, the spatially integrated fourth-order space/retarded-time covariances, which are used in the models, are instead very well fitted by Gaussian functions of different widths for different components, which is counter to conventional modeling practice. We also examine the components of Lighthill's analogous noise source that are linear and quadratic in velocity fluctuations, as well as components that are deviations from $p'=a_\infty^2\rho'$. The spectrum from the linear components is more peaked and more direction dependent than the spectral shape of the quadratic component's noise, which is relatively independent of angle. These two components are also correlated, especially at small angles where their mutual correlation coefficient reaches as low as -0.4, which casts doubt on models that treat these so-called shear noise (linear) and self-noise (quadratic) terms as distinct. The $p'-a_\infty^2\rho'$ contribution is relatively small, but not negligible as might be expected for this nearly isothermal jet. The total radiated power of the quadratic terms is nearly the same as that of all components combined. It is shown that the standard Lighthill framework does not lead to a straight forward designation of what noise comes from what region of the jet. © *2003 American Institute of Physics.* [DOI: 10.1063/1.1569919]

I. BACKGROUND AND OBJECTIVES

A key difficulty in modeling jet noise is the complexity of the turbulence statistics involved. Unlike Reynolds stress models, which have been relatively successful, turbulence as a source of noise is typically a higher order statistic (fourth instead of second), nonlocal, and necessarily time (or retarded time) dependent. Expressions for the far-field noise often involve the integrated fourth-order space/retarded-time covariance of velocity fluctuations. These are at the core of statistical models of jet noise based on both the Lighthill[1–3] and Lilley[4–7] equations. Complete measurements of the necessary statistics have eluded experimentalists so assumptions made in formulating models remain untested. Typically, normal distributions[1,4,8] are assumed for the turbulence fluctuations so that the fourth-order quantities can be computed in terms of second-order statistics, which are more easily measured and modeled. The retarded time dependence of the integrated correlation must also be assumed. Both Gaussian and exponential forms have both been used, with an exponential sometimes selected to better represent the spectral characteristics of the computed sound,[4] but there is no real basis for this because the integrated correlations have never before been computed.

Our first task is to compute these integrated correlations. We use an existing well validated simulation database of a turbulent jet. The database is discussed in Sec. II and the turbulence statistics in question are discussed in Sec. III.

Several attempts to model jet noise[1,2,4–7] have followed the standard Reynolds decomposition of the flow variables: $q=\overline{q}+q'$, where q is a flow quantity and $\overline{q}$ and q' are its average and an instantaneous perturbation. Our second task is to use the same simulation database to examine this decomposition in the context of jet noise. We focus on how it is typically used in jet noise models utilizing Lighthill's theory.

Lighthill's equation[9] can be written

$$\frac{\partial^2\rho'}{\partial t^2}-a_\infty^2\frac{\partial^2\rho'}{\partial x_j\partial x_j}=\frac{\partial^2 T_{ij}}{\partial x_i\partial x_j}, \tag{1}$$

where $T_{ij}=\rho u_i u_j+(p-a_\infty^2\rho)\delta_{ij}-\tau_{ij}$ is the Lighthill stress tensor, a_∞ is the ambient sound speed, τ_{ij} is the viscous stress, and ρ' is a density fluctuation. The double divergence of T_{ij} appearing on the right-hand side of (1) serves as a nominal acoustic source, but its use here should not be interpreted in any way as an attempt to define the true noise source in the jet. Such an interpretation would be misguided for at least two reasons. The first, which has been well understood starting with Lighthill's original derivation of (1), is that all effects aside from propagation in a homogeneous stationary medium, such as refraction, are lumped into this nominal source. More sophisticated theories, such as acoustic analogies based on the Lilley equation, attempt to treat mean-flow refraction explicitly,[10–12] but are more analytically challenging. We focus on the Lighthill theory in this part of the paper because it remains a popular modeling approach and because we have a reliable means of computing the far-field sound associated with its different near-field

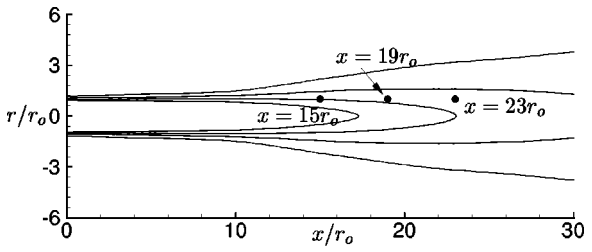

FIG. 1. Schematic showing points used relative to mean velocity with evenly spaced contours between $0.1U_j$ and $0.7U_j$. All are coincident with the nozzle lip at $r=r_0$.

components. The second reason is that most of $T_{ij,ij}$ does not radiate to the far acoustic field, which is also widely understood. What $T_{ij,ij}$ does provide is an exact connection between near-field turbulence statistics and their noise. This is how we use it.

Applying the Reynolds decomposition to T_{ij} gives

$$T_{ij}=\bar{T}_{ij}+\underbrace{\rho(\bar{u}_i u_j'+u_i'\bar{u}_j)}_{\text{shear}}+\underbrace{\rho u_i' u_j'}_{\text{self}}+\underbrace{(p'-a_\infty^2\rho')\delta_{ij}}_{\text{entropic}}-\underbrace{\tau_{ij}'}_{\text{viscous}}, \tag{2}$$

where following common practice source terms that are linear in the fluctuating velocities have been labeled shear to reflect that this source component entails turbulent fluctuations interacting with the sheared mean flow, and source terms that are quadratic in the fluctuating velocities have been labeled self to reflect that this source component entails turbulent fluctuation interacting with themselves. For clarity we have not yet decomposed ρ into $\overline{\rho}$ and ρ'. The so-called entropic contribution has often been neglected to facilitate analysis,[9,13] but is thought by some to be significant for both hot and cold jets, having an efficient dipole component.[3,12] Lighthill[9] stated emphatically that the viscous component of T_{ij} could be neglected with respect to the far-field sound, and this view has held.[12,13] An implicit result of Colonius and Freund's[14] computation of jet noise using Lighthill's analogy was that τ_{ij} does not contribute substantially even at Re $=2000$.

Until now, there has been no direct measurements to verify the modeling of different components, only of the net result. A common modeling assumption is that the self-noise and shear noise contributions are independent, the validity of which is untested. We also use the simulation database to directly evaluate the role of the different components. The details of the specific decomposition used are provided in Sec. IV. The method used to compute the far-field sound is presented in Sec. V. Results concerning directivity, source compactness, and the spectral contributions of different components are presented in Secs. VI–VIII.

II. SIMULATION DATABASE

The database we use was reported on in detail by Freund.[15] It is a Mach 0.9, Reynolds number 3600, constant stagnation temperature ($T_j/T_\infty=0.86$) jet. It has been validated against the corresponding experimental results of Stromberg,[16] matching the mean flow development, sound pressure level directivity at $60r_0$ (60 jet radii) from the nozzle, and sound spectrum at $\alpha=30°$ measured from the

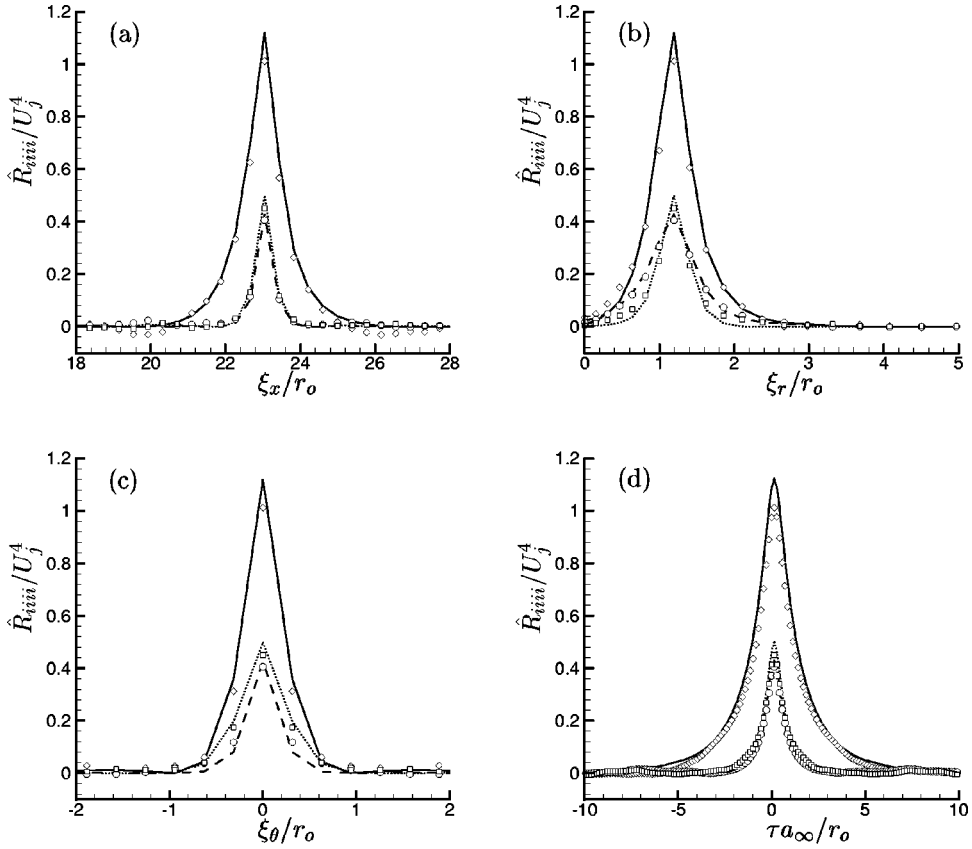

FIG. 2. Direct evaluation of (6) for normal components at $x=23r_0$ and $r=1.1r_0$. The lines are $\hat{R}_{iiii}=\overline{u_iu_i'}\,\overline{u_iu_i'}+\overline{u_iu_i'}\,\overline{u_iu_i'}$ and the symbols are $\hat{R}_{iiii}=\overline{u_iu_iu_i'u_i'}-\overline{u_iu_i}\,\overline{u_i'u_i'}$: — and ◇ are 1111, --- and ○ are 2222, and ⋯ and □ are 3333. One-dimensional offsets in (a) ξ_x, (b) ξ_r, (c) ξ_θ, and (d) τ.

downstream axis. Because of its low Reynolds number, this jet has laminar shear layers that transition before the end of the potential core. After transition, its turbulence has broad-banded energy spectra and rapidly decaying two-point correlations, and viscous dissipation is a significant component in the turbulent kinetic energy budget. Reynolds stresses and spreading rates downstream of the potential core match those measured in higher-Reynolds-number experiments.

Despite this agreement with some aspects of high-Reynolds-number turbulence, we must remain aware in interpreting our results that there are qualitative differences in the noise from a low-versus high-Reynolds-number jet. Most notably, the spectrum of a high-Reynolds-number jet is broader because of the greater range of turbulence scales in the flow. There are two general factors that might cause this. The first is that the broader local turbulence spectra leads to higher frequency noise. However, these fine scales contain relatively little energy, making it more likely that the high frequencies missing at low Reynolds numbers instead come from energetic structures in the shear layers near the nozzle, which are higher frequency by virtue of their smaller size. Indeed, Lighthill's[17] statistical analysis suggests that most of the noise comes from ''eddies only slightly smaller than the main energy bearing eddies.'' Similarly, noise source localization experiments[18] have shown that most of the high-frequency noise has an apparent origin in the thin shear layers near the nozzle. Under this interpretation, a low-Reynolds-number jet can be viewed as a model for that portion of a high-Reynolds-number jet near and beyond the close of the potential core. Some additional Reynolds number effects are discussed later in this paper and in an experimental study of Reynolds number effects by Long and Arndt.[19]

The flow simulation used $N_x \times N_r \times N_\theta = 640 \times 250 \times 160$ points in the axial, radial and azimuthal directions, respectively. Data were stored on every other mesh point in all three coordinate directions every 20 numerical time steps of $\Delta t = 0.0085 r_0 / a_\infty$ each, which corresponds to a Strouhal number St$=14.1$, well above any of our frequencies of interest in the sound field.

III. NOISE SOURCE STATISTICS

Making a compact source assumption, the radiated acoustic intensity is directly related to the volume integral of the of the space/retarded-time covariance of the Lighthill stress,

$$I(\mathbf{x}) = \frac{x_i x_j x_k x_l}{16\pi^2 a_\infty^5 |\mathbf{x}|^5} \int_\infty \int_\infty \frac{\partial^4}{\partial \tau^4} \overline{T_{ij}(\mathbf{y},t) T_{kl}(\mathbf{y}+\boldsymbol{\xi}, t+\tau)} d\boldsymbol{\xi}\, d\mathbf{y}, \tag{3}$$

which follows after Lighthill[9] and Ffowcs Williams[20] and was used extensively by Ribner.[1] Often in formulating statistical noise models, the stress tensors are approximated as[1]

$$T_{ij} \approx \rho u_i u_j, \tag{4}$$

which gives the sound due to a point in the flow as

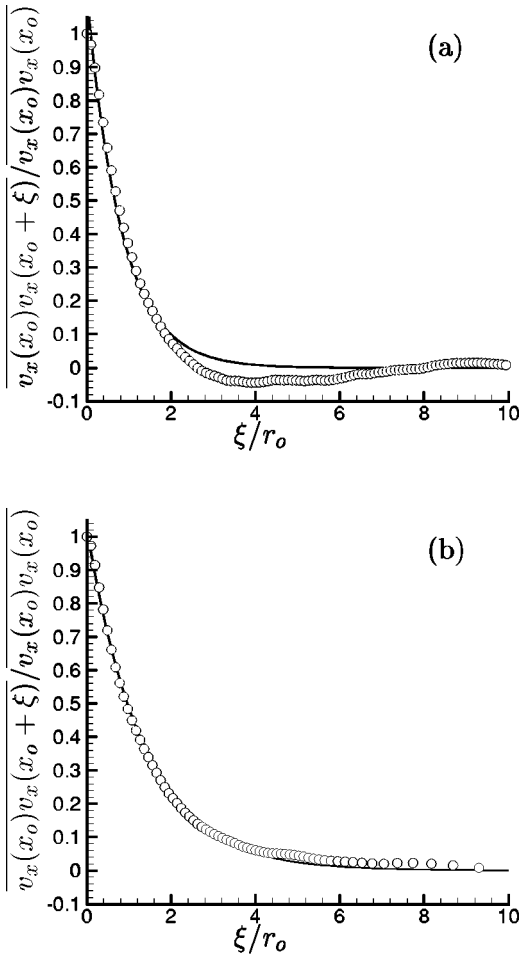

FIG. 3. Axial two-point correlation for (a) $x_0 = 19.0 r_0$ and (b) $x_0 = 26.5 r_0$ with exponential fits $\exp(-x/0.83)$ and $\exp(-x/1.34)$, respectively.

$$I^p_{ijkl} \propto \frac{\partial^4}{\partial \tau^4} \int_\infty \overline{u_i u_j u'_k u'_l}\, d\boldsymbol{\xi}, \tag{5}$$

where $u' = u(\mathbf{y}+\boldsymbol{\xi}, t+\tau)$. This formula is also the basis of some modern statistical jet noise models based on both the Lilley[4] and Lighthill[3] equations. We shall see (Sec. VI) that the $(p - a_\infty^2 \rho)$ term, which is neglected here, does indeed alter the directivity, but mostly near the jet axis. It does not contribute much to the net radiated power (Table III) or for $\alpha \gtrsim 45°$, but the peak radiation is important in some application since some regulations are based on this.

The integrated fourth-order space/retarded-time correlation (5) that constitutes the core of (3) is often simplified to facilitate the use of experimental data in tunning models. Assuming that the turbulence has a normal joint probability distribution gives[21]

$$R_{ijkl} = \overline{u_i u_j u'_k u'_l} = \overline{u_i u_j}\ \ \overline{u'_k u'_l} + \overline{u_i u'_k}\ \ \overline{u_j u'_l} + \overline{u_i u'_l}\ \ \overline{u_j u'_k} \tag{6}$$

(see Figs. 1 and 2). This is checked directly in Fig. 2 for the normal components at the points indicated in Fig. 1. Though convergence is relative poor for the fourth-order tensor, the agreement is seen to be very good, justifying the approximation in (6). It is more difficult to converge statistics for other components because the τ-dependent component, $\overline{u_i u'_k}\ \overline{u_j u'_l}$

$+\overline{u_i u_l'}\,\overline{u_j u_k'}$, is relatively smaller compared to the τ-independent component, so these are not shown. Nevertheless, our results suggest that second-order correlation statistics, which are relatively easy to measure at least in one direction, can be used in (6), a generalization of which has been provided by Lighthill.[17] Two-point correlations are known to be well fitted by exponential functions in high-Reynolds-number jets,[22] but not necessarily in low-Reynolds-number simulations of homogeneous turbulence, as discussed in the context of noise by Lilley.[23] Thus it is important to check their form here in our low-Reynolds-number jet. Figure 3 shows $\overline{v_x(x_0)v_x(x_0+\xi)}$ for $x_0=18.0r_0$ and $x_0=26.5r_0$, both at $r=r_0$, and fitted by exponential functions. The fits are good, essentially perfect at $x=26.5r_0$ where the local Reynolds number is, of course, higher. Likewise, the temporal two-point correlations are strongly peaked and also well fitted by exponentials (Fig. 4).

Of course, the acoustic intensity (3) depends upon the integrated correlation,

$$P_{ijkl}=\int_{\infty}\overline{u_i u_j u_k' u_l'}\,d\boldsymbol{\xi}, \tag{7}$$

which, based on two-point correlations, is often assumed by modelers to also have an exponential form.[4,6] However, this is not the case as seen in Fig. 5 where it is instead well fitted by Gaussian functions,

$$f(\tau)=\exp\left[-\frac{\tau^2}{\tau_0^2}\right]. \tag{8}$$

Data at $x=19r_0$, $r=1.1r_0$ are plotted in Fig. 2 and the fitting coefficients for all points in are given in Table I. As seen by the error norms given in this table, all the fits are very good. We also see that the width of the Gaussian depends on the components, with the same relative widths at the different x points. However, the τ_0 at different x do not scale well with a local time scale based on the local mean flow velocity and jet half-width, $u_c/\delta_{0.5}$, but this should not be expected since we are still so near to the end of the potential core, where the turbulence is not expected to be in equilibrium, especially in this low-Reynolds-number jet since this is also just downstream of the transition to turbulence. (We note in passing that using a fixed velocity scale and the local $\delta_{0.5}$ width of the jet to construct a local time scale does collapse the data from different x, but we see no reason to expect this in general.) To compute noise, this data is differenced in time four times, so even the small deviation from Gaussian that we see in Fig. 2 will potentially be important. Nevertheless, error for using an exponential fit for this flow would be much greater.

IV. SOURCE DECOMPOSITION

Neglecting viscosity, Lighthill's noise source is the double divergence of $T_{ij}=\rho u_i u_j+(p-a_\infty^2\rho)\delta_{ij}$, where u_i are the instantaneous velocities, and p and ρ are the instantaneous pressure and density. The source decomposition we

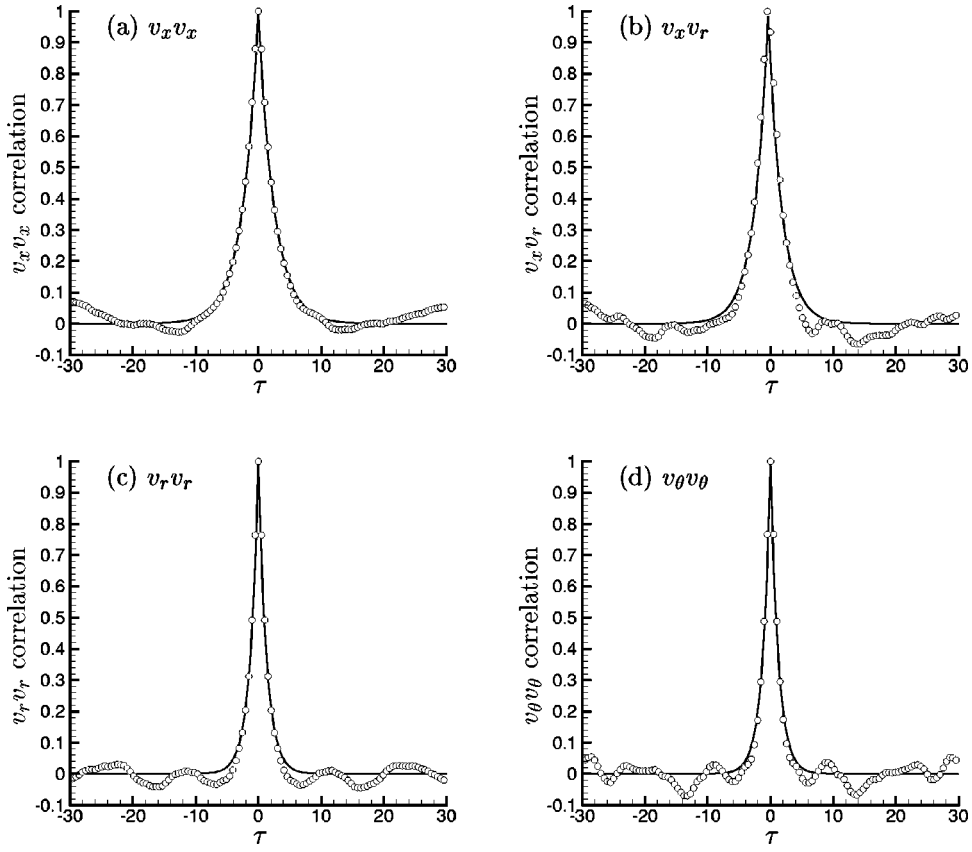

FIG. 4. Two point in time correlations, $\overline{v(t)v(t+\tau)}$, at $r=1.1r_0$ and $x=19.0r_0$. The — lines are exponential fits by $\exp(-\pi/\tau_0)$: (a) $v_x v_x$ with $\tau_0=2.54$, (b) $v_x v_r$ with $\tau_0=2.18$, (c) $v_r v_r$ with $\tau_0=1.32$, (b) $v_\theta v_\theta$ with $\tau_0=1.27$.

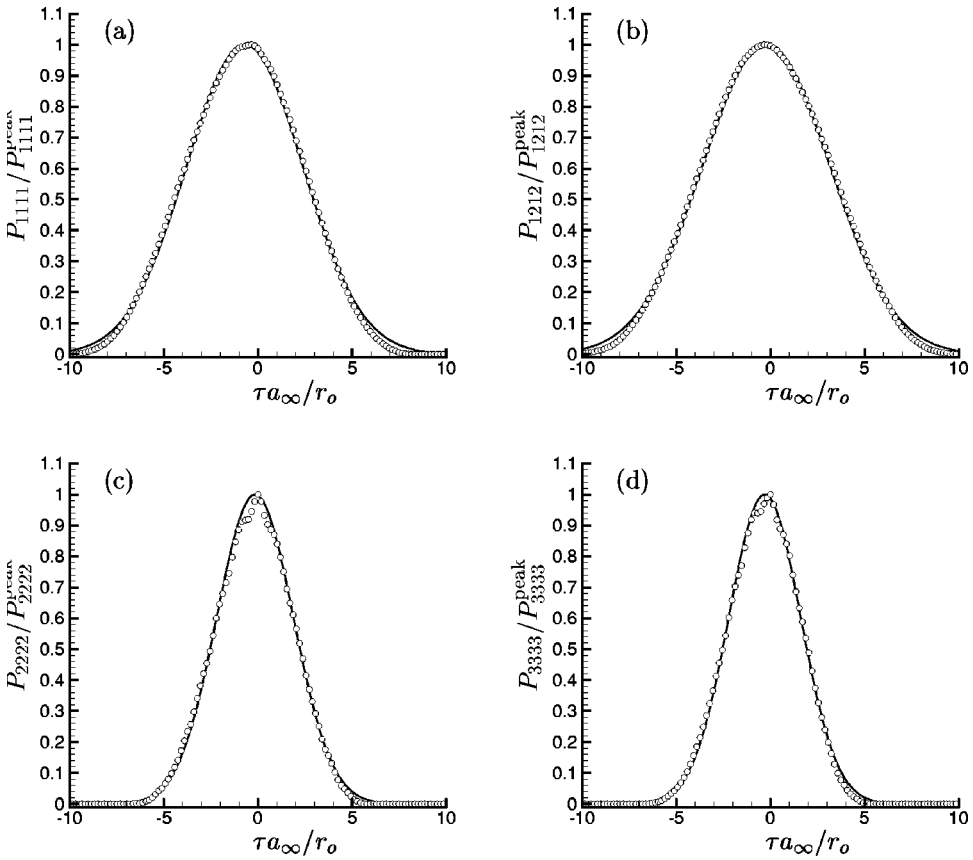

FIG. 5. Integrated fourth-order correlation tensor as defined in (7) shown with open circles ○ and Gaussian fits —. Fitting parameters are given in Table I.

consider splits T_{ij} into components that are linear, T_{ij}^l, and quadratic, T_{ij}^n, in velocity fluctuations plus the so-named entropy component, T_{ij}^s,

$$T_{ij} = \underbrace{\rho\bar{u}_i\bar{u}_j + (\bar{p} - a_\infty^2\bar{\rho})}_{T_{ij}^m} + \underbrace{\rho\bar{u}_i u_j' + \rho\bar{u}_j u_i'}_{T_{ij}^l} + \underbrace{\rho u_i' u_j'}_{T_{ij}^n} + \underbrace{(p' - a_\infty^2\rho')\,\delta_{ij}}_{T_{ij}^s}. \tag{9}$$

The mean component T_{ij}^m by definition does not make noise. We have not decomposed the density as one might into $\rho = \bar{\rho} + \rho'$ in the velocity terms, because, as seen in Table II, the sound from T_{ij} is nearly the same as that from

$$T_{ij}^{\bar{\rho}} = \bar{\rho}\bar{u}_i u_j + (p' - a_\infty^2\rho')\,\delta_{ij}. \tag{10}$$

Thus we do not discuss the explicit effect of density fluctuations in the $\rho u_i u_j$ terms.

In the spirit of Lighthill's pioneering work,[9,24] Ribner[1] made extensive use of this source decomposition. More recently this decomposition has been coupled to k-ε turbulence models as a predictive tool.[25,26] A similar decomposition into self-noise and shear noise components is also used in modeling the source terms[4,5,7,27] in the linearized Lilley equation,[11] which extends the acoustic analogy approach to explicitly include refraction.

TABLE I. Parameters for fitting with (8). E_2 is the error norm for the fit: $E_2 = r_0^{-1} a_\infty \int (f - P/P_{\max})^2\, d\tau$.

x/r_0	$ijkl$	E_2	$\tau_0 a_\infty / r_0$
15	1111	0.015	3.851
	1212	0.021	4.113
	2222	0.042	2.595
	3333	0.019	2.573
19	1111	0.028	4.379
	1212	0.025	4.809
	2222	0.032	2.866
	3333	0.022	2.690
23	1111	0.048	6.131
	1212	0.021	6.763
	2222	0.024	3.461
	3333	0.019	3.307

V. COMPUTING THE FAR-FIELD SOUND

Given T_{ij} or one of its components, the following procedure was used to compute the far-field sound. The data were first transformed in θ by

$$\tilde{T}_{ij}^{(n)}(x,r,t) = \frac{1}{N_\theta}\sum_{k=0}^{N_\theta - 1} T_{ij}(x,r,\theta_k,t)\, e^{in\theta_k} \quad \text{for } n = -N_{n_{\max}},\ldots,N_{n_{\max}}, \tag{11}$$

which was done as an efficient and accurate means of compressing the data. The stress tensor T_{ij} was rotated into cylindrical coordinates to facilitate the transform. We see in

TABLE II. Evaluation of use of $\rho u_i u_j$ for $\overline{\rho} u_i u_j$ and truncation of azimuthal Fourier series expansion. Values shown are $\overline{p'p'}/\rho_j^2 U_j^4 \times 10^{10}$ on a circular arc at $240r_0$. The numbers in parentheses, (5) and (11), are $N_{n_{\max}}$.

α	$T_{ij}(5)$	$T_{ij}(11)$	$T^{\overline{\rho}}{}_{ij}(5)$	$T^{n}{}_{ij}(5)$	$T^{n}{}_{ij}(11)$
30.00	30.45	30.74	31.81	21.45	21.65
60.00	11.00	11.33	11.32	11.14	11.35
90.00	5.66	5.99	5.84	4.93	5.10
120.00	2.99	3.09	3.17	1.56	1.61

Table II that the noise eventually computed from $N_{n_{\max}}=5$ versus $N_{n_{\max}}=11$ modes differs little, so we take $N_{n_{\max}}=5$ as sufficient.

Next, $\tilde{T}_{ij}^{(n)}(x,r,t)$ was transformed in time following a procedure similar to that we used in the past.[15] The time series at each x and r mesh point and n-mode was first multiplied by

$$w(t)=\frac{1}{2}\left[\tanh\left(5\,\frac{t-t_1}{t_1-t_0}\right)+\tanh\left(5\,\frac{t_f-t}{t_f-t_2}\right)\right], \tag{12}$$

where t_0 and t_f in (12) are the times in the simulation when it was determined to be statistically stationary and the final time, respectively. Times t_1 and t_2 are the 5% and 95% points in this time series. This contaminates the resulting noise, but only for a finite length of time that can be unambiguously identified in advance through straightforward retarded time considerations. The time transform was then

$$\check{T}_{ij}^{(n)}(x,r,\omega_m)=\frac{1}{N_t}\sum_{l=1}^{N_t} w(t_l)\tilde{T}_{ij}^{(n)}(x,r,t_l)e^{-i\omega_m t_l}$$
$$\text{for } m=-N_t/2,\ldots,N_t/2-1, \tag{13}$$

where $N_t=2304$, and the discrete angular frequencies were defined $\omega_m=2\pi m/T$, where T is the implied time period.

Finally, the data were inverse transformed in θ by

$$\hat{T}_{ij}(x,r,\theta_k,\omega_m)=\sum_{n=-N_{\theta_{\max}}}^{N_{\theta_{\max}}}\check{T}_{ij}^{(n)}(x,r,\omega_m)e^{in\theta_k}$$
$$\text{for } k=0,\ldots,N_\theta-1, \tag{14}$$

rotated into Cartesian coordinates, and convolved with the twice differentiated free-space Green's function for the Helmholtz equation to compute the acoustic pressure Fourier coefficients $\hat{p}'(\mathbf{x},\omega_m)$ at listener point $\mathbf{x}$,

$$\hat{p}'(\mathbf{x},\omega_m)=\int_\Omega \hat{T}_{ij}(\mathbf{y},\omega_m)\frac{\partial^2}{\partial x_i \partial x_j}\left[\frac{e^{-i\omega_m|\mathbf{x}-\mathbf{y}|/a_\infty}}{4\pi|\mathbf{x}-\mathbf{y}|}\right]d\mathbf{y}$$
$$\text{for } m=-N_{\omega_{\max}},\ldots,N_{\omega_{\max}}, \tag{15}$$

where we have used $\hat{p}'=a_\infty^2\hat{\rho}'$. Ω is the physically realistic region of the cylindrical simulation domain, which extended $x=31r_0$ downstream from the nozzle and out to $r=8r_0$. Taking $N_{\omega_{\max}}=327$ was sufficient to compute all frequencies up to St$=2.0$, a range which, as we shall see, constitutes most of the noise from this jet. The time-dependent pressure at point $\mathbf{x}$ is

$$p'(\mathbf{x},t_l)=\sum_{m=-N_{\omega_{\max}}}^{N_{\omega_{\max}}}\hat{p}'(\mathbf{x},\omega_m)e^{-i\omega_m t_l} \quad \text{for } l=0,\ldots,N_t-1. \tag{16}$$

Note that we have used an exact formulation, making no source compactness ($M\to 0$) assumption.

Figure 6(a) shows $p(\mathbf{x},t)$ at 30° from the jet axis and $60r_0$ from the nozzle. The region affected by the windowing procedure is evident, but constitutes less than one-quarter of the time series. There are sufficient unaffected data to converge statistics. Figure 6(b) shows the energy spectrum of the pressure fluctuations at this same point, comparing with corresponding experimental data and the spectrum at the same position computed previously using a different method.

VI. DIRECTIVITY

Figure 7 shows that the sound from the shear noise source, T_{ij}^{l}, is more directional than the self-noise source, T_{ij}^{n}, and has an angle of extinction near $\alpha=90°$. The T_{ij}^{s} term is insubstantial at large angles, but near to the down-

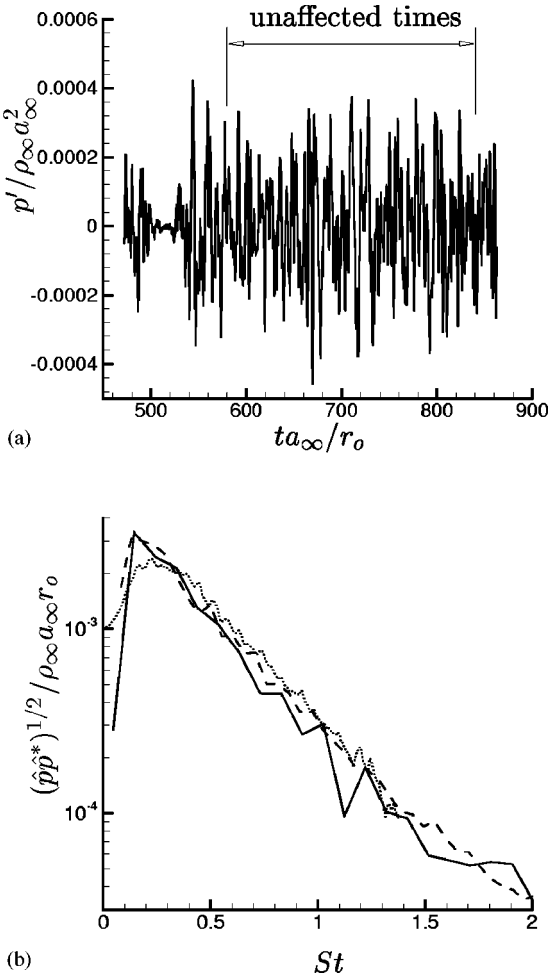

FIG. 6. Sound data at $\alpha=30°$, $60r_0$ from the nozzle. (a) Time history showing the finite period affected by the windowing procedure. (b) Time spectra, — present solution of the Lighthill equation; --- from Freund (Ref. 15); and ··· from the experiment of Stromberg *et al.* (Ref. 16). Only a relative scale was provided by Stromberg *et al.* so it has been adjusted vertically.

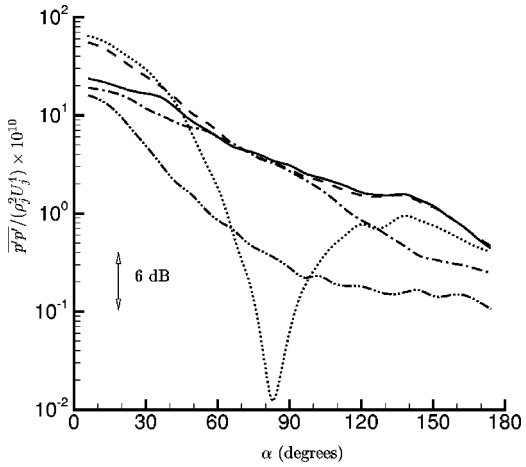

FIG. 7. Directivity on a circular arc $240r_0$ from the nozzle for components defined in (9): —, T_{ij}; ---, $T_{ij}-T_{ij}^s$; $\cdots$ T_{ij}^l; -·-, T_{ij}^n; and -···-, T_{ij}^s.

stream jet axis it is significant even though the temperature ratio of this jet is only $T_j/T_\infty=0.86$. Mitchell *et al.*[28] also found this term to be non-negligible for the noise from vortex pairing in a truly (not just in the mean) axisymmetric uniform temperature jet. The $(p'-a_\infty^2\rho')$ fluctuations are indeed the same order as the Reynolds stresses: $(p'-a_\infty^2\rho')_{\text{rms-max}}=0.079\rho_j U_j^2$, while the Reynolds stresses have peaks of $(\overline{u_x'u_x'})_{\max}\approx 0.040U_j^2$ and $(\overline{u_r'u_r'})_{\max}\approx 0.023U_j^2$, for example.

The net acoustic power (all angles) of the different components is tabulated in Table III. We see that the power from just the quadratic velocity fluctuations terms is 83% of the total, which suggests that a large part of the apparent acoustic energy due to T_{ij}^l can, in fact, potentially be interpreted as redirection by flow-acoustic interaction.

Lilley[12] finds it instructive to rewrite $p-a_\infty^2\rho$ in terms of the fluctuating total enthalpy and a kinetic energy component. Using the energy equation and the perfect gas equation of state (and integrating), it is equivalent to

$$p-a_\infty^2\rho=\underbrace{-\frac{\gamma-1}{2}\rho u^2}_{\text{Term I}}+\underbrace{a_\infty^2\int\frac{\partial}{\partial x_j}\left[\rho u_j\left(\frac{h_\infty-h_s}{h_\infty}\right)\right]dt}_{\text{Term II}}, \tag{17}$$

where h_s is the stagnation enthalpy and h_∞ is the ambient enthalpy. Lilley shows that the second Term II has a dipole form making it more acoustically efficient, which potentially explains the less-than-U^8 sound power scaling of hot jets.

TABLE III. Net radiated acoustic power.

Component	Power/$\rho_j U_j^3 A_j$	Power/power T_{ij}
T_{ij}	8.3×10^{-5}	1.00
T_{ij}^l	8.7×10^{-5}	1.05
T_{ij}^n	6.9×10^{-5}	0.83
T_{ij}^s	2.0×10^{-5}	0.25

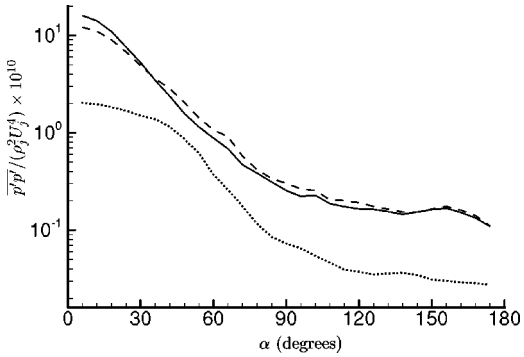

FIG. 8. Directivity on a circular arc $240r_0$ from the nozzle: — $(p-a_\infty^2\rho)$; --- Term I in (17); and $\cdots$ Term II in (17).

Here we find that it is much larger than Term I and constitutes most of the $p-a_\infty^2\rho$ term's contribution to the far-field sound (Fig. 8).

None of the profiles show a decrease in intensity near to the jet axis, as might be expected due to refraction, but a zone of silence is not expected for the total because of the limited band of frequencies in this low-Reynolds-number jet (e.g., Lush[29]). If we divide the data into higher and lower frequency components, we see the expected behavior (Fig. 9). (We cannot effectively analyze band-limited spectral components like Lush since we do not have sufficient data to converge statistics in frequency bands.) Low frequencies are more intense along the axis, which Goldstein[30] suggests is a low-frequency flow acoustic interaction, and high-frequency noise is reduced near the jet axis, as expected for refraction. So there is significant evidence of refraction, but we note that since the source is only evaluated for $x<31r_0$ any refraction down stream of this point is omitted. This omitted part will be relatively less effective at refracting the sound because the Mach number and shear are substantially decreased here, though the cumulative effect of a long travel distance through the shear flow might still be substantial.

It is clear in Fig. 7 that some individual components are more intense than the total, which means that the noise from

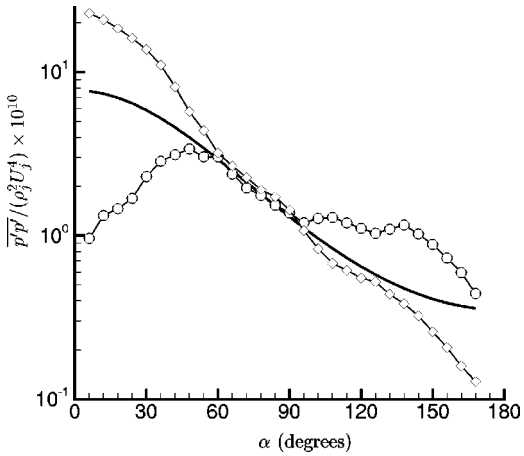

FIG. 9. Directivity for high and low frequencies: ◇, $\text{St}<0.45(1-M_c\cos\alpha)^{-1}$; ○, $\text{St}>0.45(1-M_c\cos\alpha)^{-1}$. The — line is $(1-M_c\cos\alpha)^{-5}$ with $M_c=0.3$ (see text).

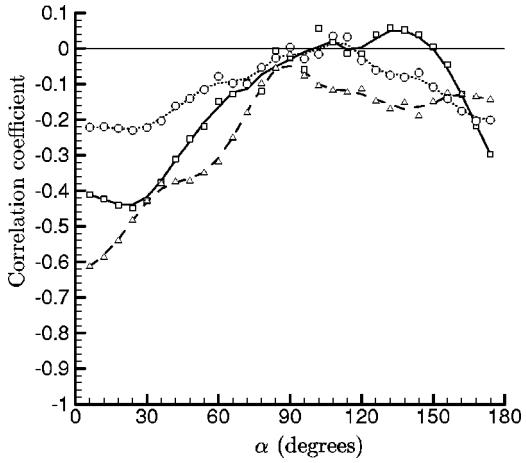

FIG. 10. Correlation coefficients defined by (18): □, C_{ln} with smoothed profile —; △, C_{ls} with smoothed profile ---; and ○, C_{ns} with smoothed profile ⋯.

the different components is correlated, significantly so given the amount of cancellation evident. To quantify the observed correlation, we define a correlation coefficient as

$$C_{\beta\gamma}=\frac{\overline{p^{\beta}p^{\gamma}}}{p^{\beta}_{\rm rms}p^{\gamma}_{\rm rms}}, \tag{18}$$

where β and γ are n, l, or s to indicate the noise from different source contributions defined in (9). C_{ls}, C_{ln}, and C_{ns} are plotted in Fig. 10. All pairs are most correlated at small angles and for the most part are canceling. At very small angles, the entropic contribution cancels the noise due to T^l_{ij} with correlation coefficient $C_{ls}\approx -0.6$. Some degree of correlation has been deduced from experimental observations of hot supersonic jets,[31] but it does not appear to have been anticipated to this degree for a nearly uniform temperature subsonic jet. The linear and quadratic velocity fluctuation contributions are also correlated at small angles, though they are often assumed to be decorrelated in models.[1,4,25] The noise from source components that are quadratic in the velocity fluctuations are relatively mildly correlated with the entropic noise. All correlations decrease to near zero by $\alpha=90°$. It is not possible to distinguish correlation due to flow acoustic interactions, which would occur say if T^l_{ij} acts to refract noise generated by T^n_{ij}, from actual noise source correlation.

Ribner[1] predicted that five inverse Doppler factors[20] would set the directivity of the velocity components of the source, with an additional factor of $\cos^4\alpha+\cos^2\alpha$ for the T^l_{ij} component. Figure 11(a) shows the self-noise component. It is significantly less directional than five inverse Doppler factors would have it for $M_c\equiv U_c/a_\infty=0.6U_j/a_\infty=0.5$. However, Freund[15] showed that the wave-number/frequency makeup of the full Lighthill source for this jet had a dominant phase Mach number of $M_c\approx 0.3$, which is indeed a somewhat better fit for the data closer to the downstream jet axis.

Modifying the Doppler factor to account for source noncompactness after Ffowcs Williams[20] or Ribner[32] gives directivity

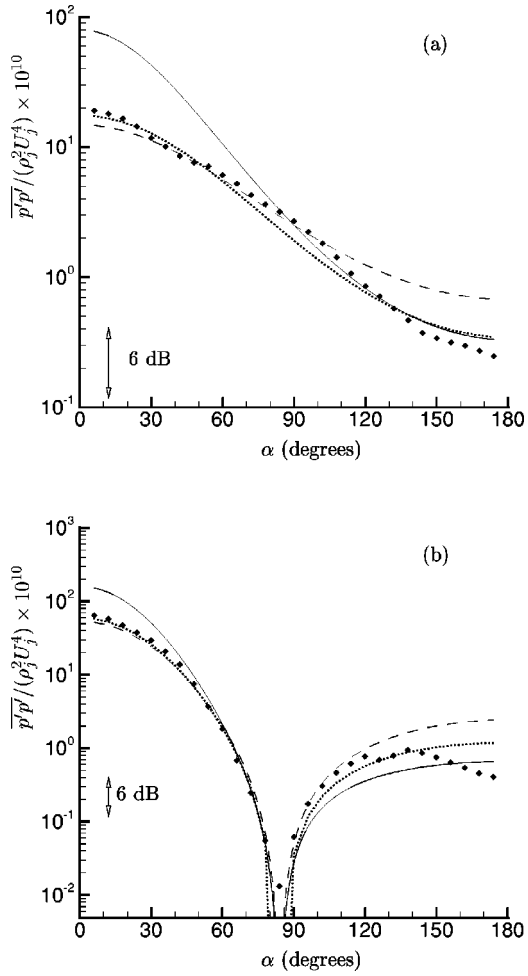

FIG. 11. Directivity on a circular arc $240r_0$ from the nozzle. (a) ◆, T^n_{ij}; —, $2.5(1-0.5\cos\alpha)^{-5}$; ---, $2.5(1-0.3\cos\alpha)^{-5}$; ⋯, $3.5[(1-0.5\cos\alpha)^2+(\omega_0\ell/c_\infty)^2]^{-5/2}$; (b) ◆, T^l_{ij}, —, $2.5(\cos^4\beta+\cos^2\beta)(1-0.5\cos\beta)^{-5}$; ---, $4.5(\cos^4\beta+\cos^2\beta)(1-0.3\cos\beta)^{-5}$. ⋯, $6.0(\cos^4\beta+\cos^2\beta)[(1-0.5\cos\alpha)^2+(\omega_0\ell/c_\infty)^2]^{-5/2}$; angle β is defined based on an origin at $x=20r_0$, which is presumably closer the center of the apparent source location. ω_0 and ℓ are defined in the text.

$$D\propto[(1-M_c\cos\alpha)^2+a^2M_c^2]^{-5/2}, \tag{19}$$

where Ribner[1] finds $a=0.55$ gives the best fit to his data. An alternate form for the added term is $(\omega_0\ell/c_\infty)^2$, where ω_0 and ℓ are a characteristic angular frequency and length scale of the radiating turbulence. For St$=0.2$, which is the peak radiated frequency and for $\ell=r_0$, which is suggested by the correlations in Fig. 2, we see that the directivity is well predicted. These parameter corresponds to $a=0.74$ in (19) which is not too different than Ribner's[1] fit.

Accounting for refraction by the mean flow in the high-frequency limit, Goldstein shows that three inverse Doppler factors are actually to be expected, which is also closer to what is observed than five Doppler factors, but since the mean velocity profile does not appear in the solution for the source T^n_{ij}, interactions with the mean flow leading to refraction are not a viable explanation in this particular case. A possibility is that the emitted directivity of five inverse Doppler factors is made more uniform by interaction with turbulence rather than the mean, which would be included as an

artificial source in T_{ij}^n. Such a change of directivity has been suggested based on qualitative analysis of this database,[33] but has not been demonstrated quantitatively for the frequencies and source locations present.

For the shear noise, the observed angle of extinction matches well with Ribner's theory if the effective source location is shifted to $x=20r_0$ [Fig. 11(b)]. Again, $M_c=0.3$ yields a better fit than $M_c=0.5$ and the noncompact correction (19) improves agreement. Ribner[1] predicted that the shear noise would be 3 dB higher than the self-noise on axis, but we observe nearly 6 dB difference. Nonetheless, the agreement is encouraging.

VII. QUADRUPOLE CHARACTER

The approach taken to solve for the far-field noise described in Sec. V, specifically the choice of convolving T_{ij} with the twice-differentiated Green's function $G_{,ij}$ for the free-space homogeneous reduced wave equation, was made to reduce numerical errors. The $T_{ij}*G_{,ij}$ convolution is, of course, mathematically equivalent to $T_{ij,ij}*G$. However, based on Lighthill's theory, we anticipated that the noise sources should have a quadrupole character whose near total cancellations would challenge the fidelity of the numerical differentiation of T_{ij} and the quadrature. Crighton[34] anticipated that small errors in such a calculation could disrupt cancellations and thereby overwhelm the physically realistic noise. Indeed, we were not able to successfully compute the far-field noise by summing up the monopoles directly. (The principal difficulty appeared to be in the accurate computation double-divergence operation on the reduced every-other-mesh-point mesh.) In our $T_{ij}*G_{,ij}$ approach, we find negligible sensitivity to how the downstream and upstream boundaries are treated, and good agreement with other methods for computing the far-field noise from this simulation.[15] This success suggests that quadrupole-like cancellations are important, but we cannot conclude directly that the sources are well modeled by point quadrupoles.

Designating a type of noise source for a turbulent jet is difficult because it is a distributed source, while concepts like quadrupole are best defined for point sources. Lighthill points out[35] that treatment of finite Mach number jets by his complete theory, of which we use only a formulation that is exact for finite Mach number to compute the far-field sound, is an extrapolation of a $M\to 0$ (point source) theory and therefore subject to certain caveats. However, we can qualify the degree to which non-point-quadrupole cancellation play a role. If the noise depends only on quadrupole cancellations, we should be able to add up the directivities of different physical regions of the jet without missing cancellation, which would be attractive from a modeling perspective because it would allow us to define the noise from a part of the jet, such as a particular streamwise slice. However, if non-point-quadrupole cancellation are substantial, we will not be able to make such a definition.

The noise from several different downstream cylindrical sections of the jet are plotted in Fig. 12(a). We see that the noise from each is actually much louder than the total. There are substantial nonquadrupole cancellation that are disrupted

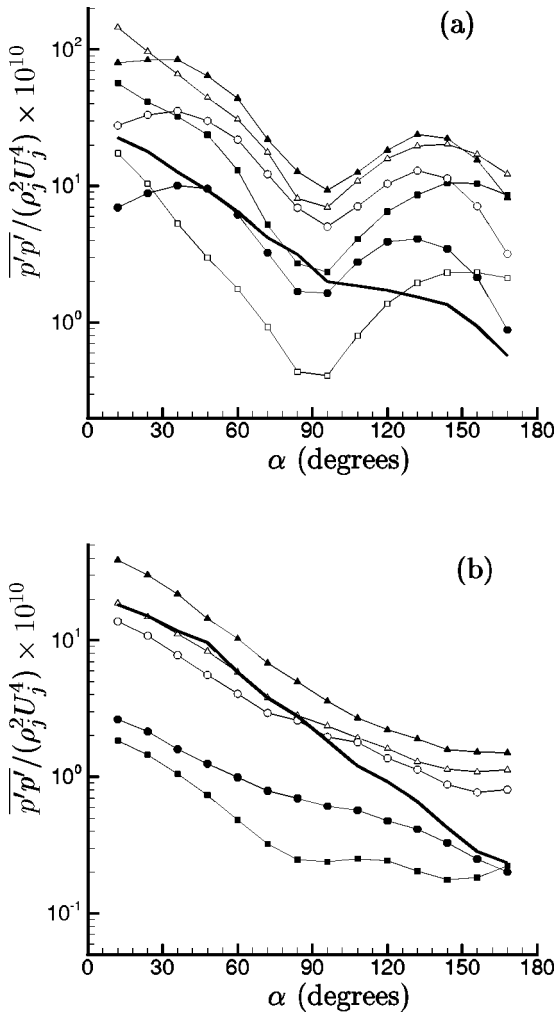

FIG. 12. The effective directivity of streamwise portions of the jet as defined by dividing (15) into sub-integrals in x: (a) T_{ij} and (b) T_{ij}^n, where symbols are $0\leqslant x\leqslant 5r_0$, □ [below scale in part (b)]; $5r_0\leqslant x<10r_0$, ■; $10r_0\leqslant x<15r_0$, △; $15r_0\leqslant x<20r_0$, ▲; $20r_0\leqslant x<25r_0$, ○; and $25r_0\leqslant x<30r_0$, ●. The — line is the total.

when the integral (15) is split in x. This result is congruous with different observations made in a previous study of this database which suggested a nonquadrupole character for the sources.[15] There it appeared that the dominant structure of the Lighthill source at certain frequencies was a noncompact wave packet, though flow acoustic interactions might increase the apparent size of the source. Figure 12(b) shows the noise from these same downstream regions for just the T_{ij}^n part of the source, so there is no mean-flow acoustic interaction in this solution. We see that the non-point-quadrupole effect is less pronounced than for the full source, but that it is still significant.

VIII. TIME SPECTRA

All the components contribute to the far-field sound over a range of frequencies, but their spectral shapes differ and, for some, are strongly dependent on α. Figure 13 shows far-field noise spectra at four different angles. Closest to the jet at $\alpha=30°$ [Fig. 13(a)], the low frequency noise is primarily due to T_{ij}^l. The noise from just T_{ij}^s is small here, but

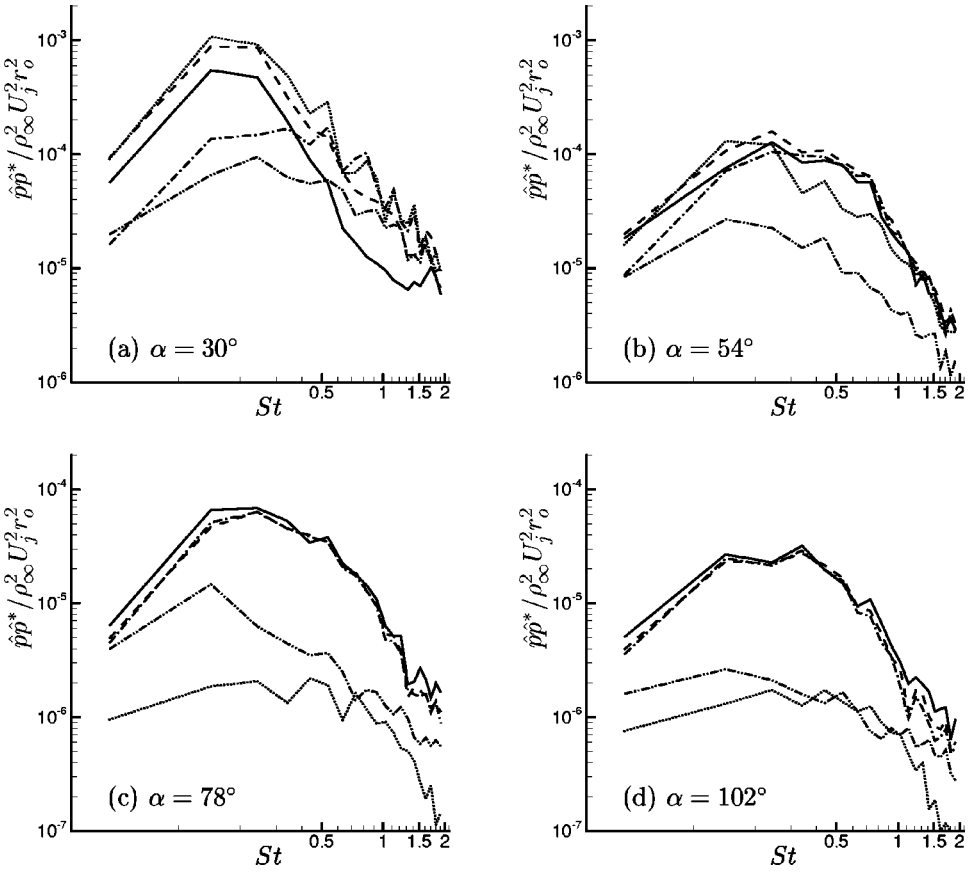

FIG. 13. Pressure spectra: —, T_{ij} total; ---, $T_{ij}^l + T_{ij}^n$ all velocity terms; $\cdots$, T_{ij}^l velocity terms linear in fluctuations; -·-, T_{ij}^n velocity terms nonlinear in fluctuations; and -···- T_{ij}^s entropy term.

because it is so highly anticorrelated with that from T_{ij}^l it cancels a portion of the T_{ij}^l noise. By itself, the noise from T_{ij}^n at higher frequencies is comparable to that just from T_{ij}^l. At $\alpha = 54°$ [Fig. 13(b)], the noise from T_{ij}^l makes of the greater part of the total noise for $\mathrm{St} < 0.3$ (though still somewhat canceled by the noise from T_{ij}^s) whereas the noise from T_{ij}^n is more significant for $\mathrm{St} > 0.3$. Both have similar levels for $\mathrm{St} \gtrsim 0.8$. At $\alpha = 78°$ and 102° [Figs. 13(c) and 13(d)], the noise from T_{ij}^n and T_{ij} are essentially the same.

Figure 14 illustrates how the spectral shape of the different components change with α. The spectrum from the full source T_{ij} clearly becomes broader with increasing α [Fig. 14(a)]. However, the spectral shape of the noise from T_{ij}^n is relatively unchanged [Fig. 14(c)]. It is the change in shape of the spectrum from T_{ij}^l and its rapidly decreasing significance near $\alpha = 90°$ [Fig. 14(b)] that accounts for most of the change of the full spectrum. The spectral peak of the noise from just T_{ij}^s [Fig. 14(d)] shifts to lower frequencies (from $\mathrm{St} \approx 0.35$ to $\mathrm{St} \approx 0.15$), but its shape is relatively broad and otherwise insensitive to α. The shifts follows the Doppler factor $(1 - M_c \cos\alpha)$ with M_c now equal to $0.6 U_j / a_\infty = 0.5$ (Fig. 15). This is surprising since we saw in the previous section that the directivity was better fitted using $M_c = 0.3$. It seems that this most intense frequency comes from the structures convecting near the end of the potential core, as suggested by visualizations.[15] This is where M_c should be closest to $0.6 U_j / a_\infty$.

Tam[36] suggests that jet noise spectra are composed of two distinct components: one due to large-scale structures and one due to so-called fine-grained turbulence. Here we see that at a fixed angle the sound from T_{ij}^n is similar to Tam's nominal fine-grained turbulence contributions, while that from T_{ij}^l, being more peaked at lower frequencies, is qualitatively similar to his nominal large-scale contribution. Unfortunately, the present jet has a Reynolds number dependent spectrum so direct comparison with Tam's empirical spectra is not instructive. However, the shear noise/self-noise decomposition is an artifact of the Reynolds average, which is made for modeling convenience, though it does seem to also divide the radiated noise into a part whose spectrum varies substantially with angle and a part that does not. But it does this without a formal splitting of the scales since all velocity fluctuations participate in both the shear noise and self-noise sources. The empirical predictive tool of Tam and Auriault[37] for the noise near $\alpha = 90°$ might be assisted by the fact the noise is, in a sense, simpler here, not depending on the mean flow through T_{ij}^l and having no substantial entropic contribution.

IX. CONCLUSIONS AND CLOSING

The implications for modeling using a shear noise, self-noise, and entropic source decomposition are clear. These contributions are highly correlated at small angles to the jet, not statistically independent as often assumed. Ribner's theory, though qualitatively correct in predicting the individual contributions of the shear noise and self-noise, especially if $M_c = 0.3$ is used to reflect the computed dominant phase velocity of T_{ij} for this jet or if the Ffowcs Williams/Ribner correction to the Doppler factor is included, but will

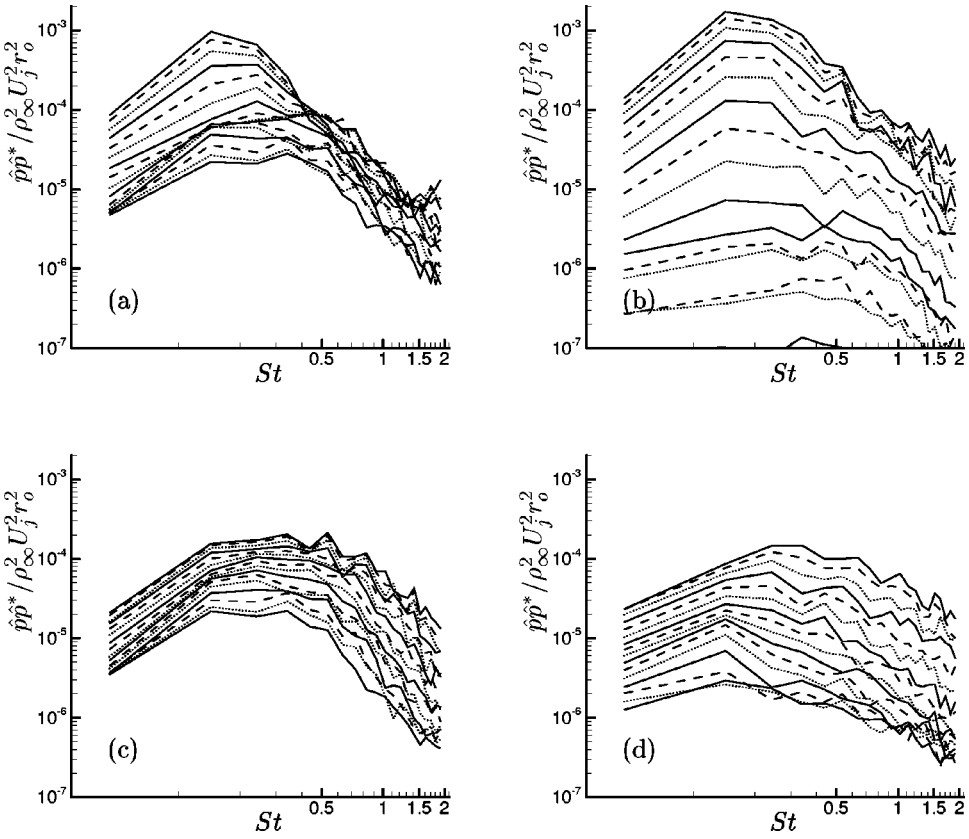

FIG. 14. Pressure spectra: (a) T_{ij} all components; (b) T_{ij}^l components linear in velocity fluctuations; (c) T_{ij}^n components quadratic in velocity fluctuations; (d) T_{ij}^s entropic component. Spectra at every 6° form $\alpha=18°$ (top curve) to $\alpha=102°$ (bottom curve) are shown.

miss their substantial mutual cancellation. Several more recent models, which have followed this same philosophy, also omit shear noise/self-noise correlation. An implication of this conclusion is that locally homogeneous turbulence, which can be used to justify the neglect of correlation between the shear noise and self-noise,[8] may not be an acceptable model for the noise source, at least at small angles to the downstream axis.

Even for this nearly uniform temperature jet, the entropic source's contribution to the far-field noise is important at small angles, especially due to its high correlation with the shear noise. Neglecting it leads to a substantial over prediction of the far-field sound. The present jet with $U_j/a_\infty = 0.83$ is close to the point where the experiments of Tanna[38] show the least sensitivity to jet temperature, so we can anticipate that this will become more significant at substantially higher or lower jet temperatures.

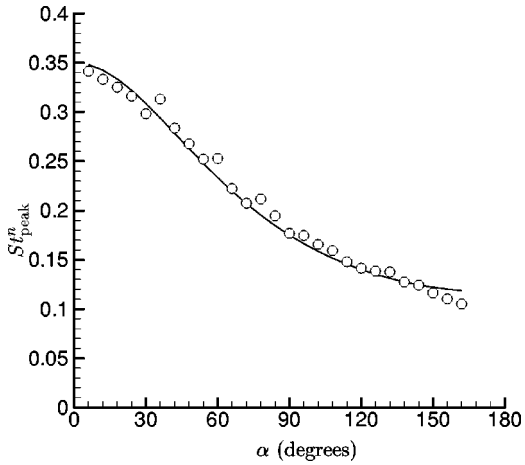

FIG. 15. Peak Strouhal number due directly to T_{ij}^n: ○ from simulation; — $0.175(1-M_c\cos\alpha)^{-1}$ with $M_c=0.6U_j/a_\infty$. The peak was determined by fitting third-order polynomials to the spectra in log–log coordinates. This removed statistical variations and provided an unambiguous recipe for determining the peak.

The sideline noise is dominated by terms in the Lighthill source that are independent of the mean flow and entropic terms. This should greatly simplify modeling for this portion of the radiated sound, perhaps making it more amenable to empirical fits.

We find that downstream of the potential core's closing two-point correlations are well fitted by exponential functions, which is characteristic of high-Reynolds-number turbulent flows. (Closer to the nozzle in the laminar/transitional shear layers they are more similar to the wavy correlations expected for flows dominated by instability waves, as expected in this region at Re=3600.[15]) The fourth-order space/retarded-time covariance tensors, which are more directly related to the far-field sound, are well approximated by the standard simplification into products of second-order correlations, which assume a normal distribution for the turbulence. However, despite the good exponential fits of the one-dimensional components, the volume integrated fourth-order correlation tensor is very well fitted by Gaussian functions, with different widths for different components. Both this functional form and the dependence on components are counter to standard modeling procedures used for statistical noise models based on Lighthill's or Lilley's equations.

It seems appropriate in closing to make a final comment

concerning the Reynolds number of the simulation used, which is low for a turbulent jet by every standard aside from modern direct numerical simulation capabilities. It is conceivable that the correlations that we observe might be an artifact of this low Reynolds number, but they are so significant that it seems unlikely that they could disappear altogether at higher Reynolds numbers. Once turbulent, the Reynolds stresses are in close agreement with jets of much higher Reynolds numbers and the two-point correlations decay rapidly, just as at higher Reynolds numbers.[15] It does not seem feasible that the energetic structures could change sufficiently with Reynolds number to display a behavior much different than we observe. What will certainly change at higher Reynolds numbers is that the near-nozzle shear layers will become turbulent. Since these eddies are relatively small, we can anticipate that they will make the high-frequency noise missing from the present simulation. Unfortunately, there does not appear to be a definitive means of directly testing these admittedly speculative assertions: we have pressed the limit of direct numerical simulation (large-eddy simulation is promising, but seems to have a resolution requirement for a high-Reynolds-number jet that is greater than the present direct numerical simulation[39]) and experimentalists have pressed the limits of their measurement techniques. Further technological advances in both might facilitate a better parametrization of Reynolds-number effects in the future and at the same time allow the details of high-Reynolds-number jet noise sources to be probed in detail as we have done here in the low-Reynolds-number limit.

ACKNOWLEDGMENTS

The author acknowledges the assistance of Devon Johnson in identifying the specific approach used to compute the far-field sound. He also thanks Professor Tim Colonius for making critical comments on an early draft of this paper. Financial support from NASA is gratefully acknowledged.

[1] H. S. Ribner, "Quadrupole correlations governing the pattern of jet noise," J. Fluid Mech. **38**, 1 (1969).
[2] T. F. Balsa, "The acoustic field of sources in shear flow with application to jet noise: convective amplification," J. Fluid Mech. **79**, 33 (1977).
[3] G. M. Lilley, "The radiated noise from isotropic turbulence with applications to the theory of jet noise," J. Sound Vib. **190**, 463 (1996).
[4] A. Khavaran, "Role of anisotropy in turbulent mixing noise," AIAA J. **37**, 832 (1999).
[5] A. Khavaran, "Influence of mean-density gradient on small-scale turbulence noise," Sixth AIAA/CEAS Aeroacoustics Conference, Lahaina, Hawaii, AIAA Pap. 2000–2059 (2000).
[6] A. Khavaran, J. Bridges, and J. B. Freund, "A parametric study of fine-scale turbulence mixing noise," AIAA Pap. 2002–2419 (2002).
[7] C. Bailly, P. Lafon, and S. Candel, "Subsonic and supersonic jet noise predictions from statistical source models," AIAA J. **35**, 1688 (1997).
[8] M. E. Goldstein and B. M. Rosenbaum, "Effect of anisotripic turbulence on aerodynamic noise," J. Acoust. Soc. Am. **54**, 630 (1973).
[9] M. J. Lighthill, "On sound generated aerodynamically: I. General theory," Proc. R. Soc. London, Ser. A **211**, 564 (1952).
[10] G. M. Lilley, "On the noise from jets," Technical Report No. CP-131, AGARD, 1974.
[11] M. E. Goldstein, *Aeroacoustics* (McGraw-Hill, New York, 1976).
[12] G. M. Lilley, "Jet noise: Classical theory and experiments," in *Aeroacoustics of Flight Vehicles*, edited by H. Hubbard (Acoustical Society of America, New York, 1995), pp. 211–289.
[13] D. G. Crighton, "Basic principles of aerodynamic noise generation," Prog. Aerosp. Sci. **16**, 31 (1975).
[14] T. Colonius and J. B. Freund, "Application of Lighthill's equation to a Mach 1.92 turbulent jet," AIAA J. **38**, 368 (2000).
[15] J. B. Freund, "Noise sources in a low-Reynolds-number turbulent jet at Mach 0.9," J. Fluid Mech. **438**, 277 (2001).
[16] J. L. Stromberg, D. K. McLaughlin, and T. R. Troutt, "Flow field and acoustic properties of a Mach number 0.9 jet at a low Reynolds number," J. Sound Vib. **72**, 159 (1980).
[17] M. J. Lighthill, "An estimate of the covariance of T_{xx} without using statistical assumptions," Appendix 1 of "On the noise radiated from a turbulent high speed jet," by G. M. Lilley, in *Computational Aeroacoustics*, edited by J. C. Hardin and M. K. Hussaini (Springer-Verlag, New York, 1992).
[18] S. Narayanan, T. Barber, and D. Polak, "High subsonic jet experiments. Part II: Turbulence and noise generation studies," AIAA/CEAS Aeroacoustics Conference and Exhibit, 6th, Maui, AIAA Pap. 2000–2023 (2000).
[19] D. F. Long and R. E. A. Arndt, "Jet noise at low Reynolds number," AIAA J. **22**, 187 (1984).
[20] J. E. Ffowcs Williams, "The noise from turbulence convected at high speed," Philos. Trans. R. Soc. London, Ser. A **255**, 469 (1963).
[21] G. K. Batchelor, *The Theory of Homogenous Turbulence* (Cambridge University Press, Cambridge, 1960).
[22] J. Bridges and M. P. Wernet, "Turbulence measurents of separated flow nozzles with mixing enhancement features," AIAA Pap. 2002–2484 (2002).
[23] G. M. Lilley, "The radiated noise from isotropic turbulence revisited," ICASE Report No. 93-75, 1993.
[24] M. J. Lighthill, "On sound generated aerodynamically: II. Turbulence as a source of sound," Proc. R. Soc. London, Ser. A **222**, 1 (1954).
[25] C. Bailly, P. Lafon, and S. Candel, "Computation of subsonic and supersonic jet mixing noise using a modified k-ε model for compressible free shear flows," Acta Acust. (Beijing) **2**, 101 (1994).
[26] W. Béchara, P. Lafon, C. Bailly, and S. Candel, "Application of the k-ε turbulence model to the prediction of noise from simple and coaxial free jets," J. Acoust. Soc. Am. **97**, 3518 (1995).
[27] A. Khavaran, E. A. Krejsa, and C. M. Kim, "Computation of supersonic jet mixing noise for an axisymmetric convergent-divergent nozzle," J. Aircr. **31**, 603 (1994).
[28] B. E. Mitchell, S. K. Lele, and P. Moin, "Direct computation of the sound generated by subsonic and supersonic axisymmetric jets," Technical Report No. TF-66, Stanford University, Mechanical Engineering, 1995.
[29] P. A. Lush, "Measurements of subsonic jet noise and comparison with theory," J. Fluid Mech. **46**, 477 (1971).
[30] M. E. Goldstein, "The low frequency sound from multipole sources in axisymmetric shear flows, with applications to jet noise," J. Fluid Mech. **70**, 595 (1975).
[31] H. K. Tanna, M. J. Fisher, and P. D. Dean, "Effects of temperature on supersonic jet noise," AIAA Pap. 73–991 (1973).
[32] H. S. Ribner, "The generation of sound by turbulent jets," Adv. Appl. Mech. **8**, 103 (1964).
[33] J. B. Freund and T. G. Fleischman, "Ray traces through unsteady jet turbulence," Int. J. Aeroacoustics **1**, 83 (2002).
[34] D. G. Crighton, "Goals for computational aeroacoustics," in *Computational Acoustics: Algorithms and Applications* (North-Holland, Amsterdam, 1988), pp. 3–20.
[35] M. J. Lighthill, "Jet noise," AIAA J. **1**, 1507 (1963).
[36] C. K. W. Tam, "Jet noise: since 1952," Theor. Comput. Fluid Dyn. **10**, 393 (1998).
[37] C. K. W. Tam and L. Auriault, "Jet mixing noise from fine-scale turbulence," AIAA J. **37**, 145 (1999).
[38] H. K. Tanna, "An experimental study of jet noise. Part I. Turbulent mixing noise," J. Sound Vib. **50**, 405 (1977).
[39] J. B. Freund and S. K. Lele, "Computer simulation of high speed jets and their noise," in *High Speed Jet Flows: Fundamentals and Applications*, edited by G. Raman, D. K. McLaughlin, and P. J. Morris (Taylor & Francis, New York, 2002).